Riccati-less approach for optimal control and estimation: an application to two-dimensional boundary layers

Onofrio Semeraro[1],†**, Jan O. Pralits**[2]**, Clarence W. Rowley**[3] **and Dan S. Henningson**[1]

[1]Linné Flow Centre, KTH Mechanics SE-100 44 Stockholm, Sweden
[2]DICCA - Universitá degli studi di Genova I-161 45, Genova, Italy
[3]MAE Department, Princeton University, Princeton, NJ 08544, USA

The control of Tollmien–Schlichting waves in a two-dimensional boundary layer is analysed using numerical simulations. Full-dimensional optimal controllers are used in combination with a setup of spatially localized inputs (actuator and disturbance) and outputs (sensors). The *adjoint of the direct-adjoint* (ADA) algorithm, recently proposed by Pralits & Luchini (In *Seventh IUTAM Symposium on Laminar–Turbulent Transition* (ed. P. Schlatter & D. S. Henningson), vol. 18, 2010, Springer), is used to efficiently compute an optimal controller known as a linear quadratic regulator; the method is iterative and allows one to bypass the solution of the corresponding Riccati equation, which is infeasible for high-dimensional systems. We show that an analogous iteration can be made for the estimation problem; the dual algorithm is referred to as *adjoint of the adjoint-direct* (AAD). By combining the solutions of the estimation and control problem, full-dimensional linear quadratic Gaussian controllers are obtained and used for the attenuation of the disturbances arising in the boundary layer flow. The full-dimensional controllers turn out to be an excellent benchmark for evaluating the performance of the optimal control/estimation design based on reduced-order models. We show under which conditions the two strategies are in perfect agreement by focusing on the issues arising when feedback configurations are considered. An analysis of the finite-amplitude disturbances is also carried out by addressing the limitations of the optimal controllers, the role of the estimation, and the robustness to the nonlinearities arising in the flow of the control design.

Key words: boundary layers, control theory, flow control

---

1. Introduction

Control of wall-bounded transitional flows might lead to high potential benefits and outcomes; for instance, even a small reduction of aerodynamic drag can greatly

---

† Email address for correspondence: onofrio@mech.kth.se

reduce the operational cost of commercial aircraft or cargo ships. In the last decade, active and passive control strategies have been investigated, in order to favourably manipulate flows. Passive control has been implemented by introducing roughness elements (White & Saric 2000) or riblets (Bechert & Bartenwerfer 1989; Luchini, Manzo & Pozzi 1991; Choi, Moin & Kim 1993), while active means include open-loop strategies, like opposition control (Hammond, Bewley & Moin 1998) or moving walls (Quadrio & Ricco 2004), as well as techniques based on control theory or adjoint-based optimization (Abergel & Temam 1990; Bewley, Moin & Temam 2001; Corbett & Bottaro 2001).

More specifically, linear control can be used to attenuate perturbations arising during the early stages of transition to turbulence, whose evolution is typically governed by linear mechanisms (Schmid & Henningson 2001); however, the design of high-dimensional controllers remains a computational challenge. Indeed, even though it is relatively common to deal with numerical simulations with dimensions $n > 10^5$, control design tools become infeasible for much smaller dimensions. For instance, linear optimal controllers are usually designed by solving a Riccati equation (Lewis & Syrmos 1995), a quadratic matrix equation that becomes computationally intractable for $n > 10^3$ (Benner, Li & Penzl 2008).

1.1. *Design-then-reduce versus reduce-then-design*

A common approach to this computational challenge is to use a reduced-order model: one identifies a simpler model, with dimension $r \ll n$, which captures the essential features of the original system to be controlled (usually referred to as the *plant*). Once such a model is available, a low-order controller can be designed using traditional methods such as Riccati solvers. This approach is usually referred to as *reduce-then-design* and it is schematically represented along the left-hand branch of the diagram in figure 1 (see Anderson & Liu 1989).

A reduced-order model can be built such that the dynamics of the system is analysed from measurements taken from the system. In other words, as mentioned by Bewley (2001), we seek to achieve the desired closed-loop system behaviour by only using measurements (outputs), with the system excited by several input signals. This dynamics is referred to as *input–output* dynamics of the system and is usually characterized by a complexity that is smaller than the original one. This feature allows one to considerably shrink the dimensions of the dynamical system, while preserving the main dynamics for the control design. A systematic way to perform such a reduction is to use balanced truncation (Moore 1981); for a high-dimensional system, balanced truncation can be approximated using a snapshot-based algorithm proposed by Rowley (2005). This methodology is equivalent to a system identification method called the eigensystem realization algorithm (ERA) (Juang & Pappa 1985), as shown in Ma, Ahuja & Rowley (2011).

The reduce-then-design approach has been successfully employed for many flow cases, such as cavity flows by Rowley & Juttijudata (2005) and Åkervik *et al.* (2007), channel flows by Ilak & Rowley (2008) and spatially developing boundary layers in both two-dimensional (Bagheri, Brandt & Henningson 2009*a*) and three-dimensional configurations (Semeraro *et al.* 2011). More recently, system identification based on auto-regressive models (ARMAX) was applied by Hervé *et al.* (2012) for the control of flows over a cavity.

The second approach sketched in figure 1 is referred to as *design-then-reduce*; in this case, a full-dimensional controller is designed first, while in the second step, the dimension of the controller is reduced. Indeed, a very high-order controller is usually
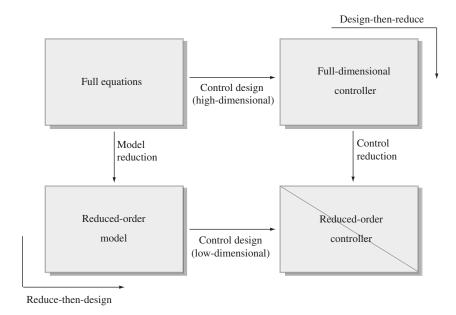
FIGURE 1. Reduction and control: the sketch represents the two approaches usually followed for the design of active controllers. In general, the two schemes do not produce equivalent results.

not of practical interest for engineering applications; thus for actual implementation, it is still important to reduce the dimension of the controller.

In general, the two approaches are not equivalent. Even though the reduce-then-design approach is quite popular in the flow control community, for the advantages already mentioned above, it has a number of drawbacks, as pointed out by Anderson & Liu (1989). First, the approximation is performed earlier in the design process, which is generally undesirable. Moreover, in order to reliably approximate the plant, some knowledge of the controller is required; but in the reduce-then-design approach, the controller is not known until the plant is reduced. In practice, the model reduction step is usually performed in open loop; when the loop is closed, a number of states disregarded during the design of the model might become important for the dynamics of the closed-loop system.

1.2. *Full-dimensional controllers and flow control*

For spatially invariant systems with distributed actuation and measurements, Bamieh, Paganini & Dahleh (2002) showed that it is possible to design spatially localized optimal controllers (or *kernels*) with a compact support in physical space. In this approach, a controller is designed for each wavenumber pair in Fourier space, independently, while the final kernel in physical space is obtained by performing an inverse Fourier transform.

This procedure has been used for plane channel flow by Högberg, Bewley & Henningson (2003) and later extended for weakly spatially developing flows by Chevalier *et al.* (2007*a*) and Monokrousos *et al.* (2008). Apart for the limit imposed by the hypothesis of spatial invariance of the system, a drawback of this methodology is the necessity of introducing a distributed system of sensors and actuators.

An alternative, more general approach to the design of optimal controllers is to compute a linear quadratic regulator by solving a Riccati equation (Lewis & Syrmos 1995). A classic technique for solution is the Chandrasekhar method, in which the full Riccati equation is replaced by a set of partial differential equations, valid when the resulting number of degrees of freedom of the system n is much larger than the number of actuators $m \ll n$. Efforts have been devoted to optimizing the integration of these equations by using Newton methods (Banks & Ito 1991) or projection on Krylov subspaces by using the Arnoldi process (see e.g. Benner 2004, and the references contained therein). An efficient solution method for this set of equations was proposed by Borggaard & Stoyanov (2008) and Akhtar *et al.* (2010), where long-time integrators are used in combination with reduced-order models based on proper orthogonal decomposition (POD).

Methods for the solution of large optimal control problems were also proposed by Bewley, Luchini & Pralits (2012), based on previous works by Bewley, Pralits & Luchini (2007) and Pralits & Luchini (2010). In particular, Bewley *et al.* (2007) presents a minimal-energy feedback control that can be obtained as a limit for $l \to \infty$, where l stands for the control penalty in a cost function to be minimized. This limitation has been circumvented in Pralits & Luchini (2010), where the *adjoint of the direct-adjoint* (ADA) algorithm was introduced and tested for the optimal control of the von Kármán street developing past a cylinder.

The original direct-adjoint optimization is replaced with the corresponding sensitivity analysis by considering the adjoint of the entire problem: this procedure changes an optimization problem of size n, the number of states, into a problem of size m, where m is the number of outputs. In flow control, usually $n \gg m$, even when multi-input–multi-output (MIMO) cases are considered (see e.g. Semeraro *et al.* 2011); moreover, the algorithm shares the same numerical machinery as the original direct-adjoint problem, making the technique particularly appealing for control design.

1.3. *Aim of the investigation*

As mentioned above, the steps of dimension reduction and control design do not, in general, commute. Thus, one might wonder about the limitations of the reduce-then-design approach when applied to a large flow system: under what conditions do the two approaches give the same reduced-order controller? What is the limiting performance of an 'ideal' full-state optimal controller designed using the full-dimensional system?

In order to address these issues, we compare the full-dimensional control design and the corresponding design based on a reduced-order model. In particular, we use the ADA algorithm to compute a controller to suppress small-amplitude perturbations in a spatially evolving two-dimensional boundary layer on a flat plate. The investigation is performed using numerical simulations. The same test case has been used in Bagheri *et al.* (2009*a*), in which the reduce-then-design approach was adopted, by first performing a balanced truncation for the identification of a reduced-order model, followed by a low-dimensional control design using a linear quadratic Gaussian (LQG) controller. In order to provide a proper benchmark for the low-dimensional design, we extend the formulation of the ADA algorithm to the estimation problem, by performing a sensitivity analysis of the dual system. An optimal estimator can be designed by solving a feedback problem applied to the adjoint variable, thus resulting in optimization based on an *adjoint-direct* system (see Kim & Bewley 2007). This approach is deterministic; however by interpreting the weights appearing in the cost function defined for the problem as covariance of the stochastic excitation, we can
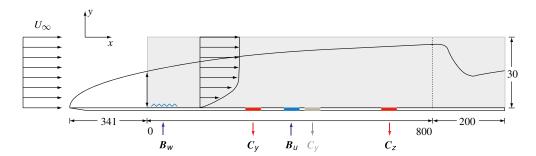
FIGURE 2. Flow case. The flow is developing over a flat plate, which physically extends to $x = 800$. The disturbance propagates from the input $\boldsymbol{B}_w$, located at $(x_w, y_w) = (35, 1)$, while the actuator $\boldsymbol{B}_u$ is placed at $(x_u, y_u) = (400, 1)$. The sensor $\boldsymbol{C}_z$ placed at $(x_z, y_z) = (750, 1)$ acts as objective function. Two locations for the estimation sensor $\boldsymbol{C}_y$ are tested: upstream of the actuator, $(x_y, y_y) = (300, 1)$, and a short distance downstream of it, $(x_y, y_y) = (405, 1)$. A fringe region extending in the interval $x \in [800, 1000]$ enforces periodicity of the solution along the streamwise direction.

easily recover the original characterization of the problem (Bagheri *et al.* 2009*b*). In the present contribution, the dual algorithm is referred to as *adjoint of adjoint-direct* (AAD).

By combining the results of the two iterative schemes, full-dimensional LQG controllers are designed. The performance of the device is investigated by a parametric analysis where the relative positions of the estimation sensor and the actuator, and the control penalty *l* are studied. Moreover, a brief investigation of the compensation of nonlinear flows is reported in order to assess the performance (and the limits) of different combinations of controllers based on the computed full-dimensional control/estimation gains.

The article proceeds as follows. First, we introduce the flow case and the input–output system in § 2. In § 3, a quick overview of the optimal control and estimation problem is presented, together with the main relations used in § 4, where the iterative procedures are outlined. Here, we summarize the ADA algorithm and introduce the AAD algorithm for the estimation problem. Results for the spatially evolving boundary layer are presented in § 5, where the evolution of small- and finite-amplitude disturbances is considered for the analysis of the control design. The conclusions are drawn in § 6.

2. Flow case

The control of small-amplitude perturbations is analysed for the two-dimensional input–output configuration already investigated by Bagheri *et al.* (2009*a*) and Belson *et al.* (2013). In figure 2, a sketch of the computational domain is shown; the streamwise and wall-normal directions are denoted by *x* and *y*, respectively.

The disturbance velocity field is governed by the Navier–Stokes equations linearized around a spatially evolving zero-pressure-gradient boundary layer flow $\boldsymbol{U}(\boldsymbol{x}) = (U, V)^{\mathrm{T}}$,

$$\frac{\partial \boldsymbol{u}}{\partial t} = -(\boldsymbol{U} \cdot \boldsymbol{\nabla})\,\boldsymbol{u} - (\boldsymbol{u} \cdot \boldsymbol{\nabla})\,\boldsymbol{U} - \boldsymbol{\nabla}p + \frac{1}{Re}\nabla^2\boldsymbol{u} + \lambda_f(x)\boldsymbol{u}, \qquad (2.1a)$$

$$0 = \boldsymbol{\nabla} \cdot \boldsymbol{u}, \qquad (2.1b)$$

$$\boldsymbol{u} = \boldsymbol{u}_0 \quad at\ t = 0. \qquad (2.1c)$$

The disturbance velocity field and the pressure field are $\boldsymbol{u}(\boldsymbol{x}, t) = (u, v)^{\mathrm{T}}$ and $p(\boldsymbol{x}, t)$, respectively, and λ_f is a parameter in a forcing term to be discussed below. The ∇ denotes the differential operator $(\partial/\partial x, \partial/\partial y)$. The Reynolds number is defined as $Re \equiv U_\infty \delta_0^*/\nu$, where δ_0^* is the displacement thickness at the inflow position, U_∞ is the uniform free-stream velocity and ν is the kinematic viscosity. For all the cases analysed in this study $Re_{\delta_0^*} = 1000$, corresponding to $Re_x \approx 3 \times 10^5$ at the computational inlet at $x = 0$.

The physical domain has dimensions $[L_x, L_y] = (1000, 30)$. No-slip conditions are imposed on the flat plate, at $y = 0$. In the free stream ($y = 30$), Dirichlet boundary conditions enforce vanishing perturbations. Periodicity is assumed along the streamwise direction within the Fourier approximation by introducing a forcing term $\lambda_f(x)\boldsymbol{u}$ in (2.1*a*); the forcing arises in a fringe region extending in $x \in [800, 1000]$ where the perturbation is forced to be zero (Nordström, Nordin & Henningson 1999).

The simulations were performed using a pseudo-spectral direct numerical simulation (DNS) code (Chevalier *et al.* 2007*b*). The spatial operators are approximated by Fourier expansion along the streamwise direction with $N_x = 768$ and $N_x = 1024$ for the linear and nonlinear cases, respectively. Chebyshev expansion in the wall-normal direction is used on $N_y = 101$ Gauss–Lobatto collocation points. Divergence-free conditions are guaranteed by the equations cast in velocity–vorticity formulation.

2.1. *Input–output system*

The first step of the control design is to specify the inputs and outputs of the *plant*, the system to be controlled. The inputs consist of an external disturbance and an actuator, whose spatial profiles are given by the matrices $\boldsymbol{B}_w \in \mathbb{R}^n$ and $\boldsymbol{B}_u \in \mathbb{R}^{n \times m}$, respectively. The number of degree of freedom of the system is $n = 2N_x N_y$, i.e. the number of grid points times the velocity components. The parameter m represents the number of actuators (for our application, $m = 1$). The outputs consist of a performance measure and a sensor, described by the matrices $\boldsymbol{C}_z \in \mathbb{R}^{k \times n}$ and $\boldsymbol{C}_y \in \mathbb{R}^{p \times n}$, respectively. The scalar value p is the number of sensors, while k is the number of outputs; also in this case, $k = p = 1$. The inputs and the outputs are shown schematically in figure 2, and described in more detail below.

Let $u(t) \in \mathbb{R}^m$ denote the control signal, and $w(t) \in \mathbb{R}$ denote an external disturbance, modelled as zero-mean, unit-variance, Gaussian white noise. The linear time-invariant system reads

$$\dot{\boldsymbol{q}} = \boldsymbol{A}\boldsymbol{q} + \boldsymbol{B}_w w + \boldsymbol{B}_u u, \tag{2.2}$$

where the matrix $\boldsymbol{A} \in \mathbb{R}^{n \times n}$ represents the linearized and discretized Navier–Stokes equations, including the boundary conditions, while the column vector $\boldsymbol{q}(t) \in \mathbb{R}^n$ indicates the velocity components of the discretized problem. Note that the time-stepper approach is used: the system matrix is never stored, but its action is approximated by marching the DNS solver in time. In this case, the storage demand in memory is of the same order as that of the flow field. The column vector $\boldsymbol{B}_w$ describes the spatial location of the disturbance, located upstream (on the left in figure 2); the impulse response of the system is shown in figure 3 where the evolving Tollmien–Schlichting (TS) wave-packet is captured at three different instants of time. The actuator $\boldsymbol{B}_u$ is modelled as a localized volume forcing close to the wall. The column vectors $\boldsymbol{B}_w$ and $\boldsymbol{B}_u$ are obtained from discretizations of the solenoidal function

$$\boldsymbol{f}(\boldsymbol{x}, \boldsymbol{x}_0) = \begin{pmatrix} \sigma_x \hat{y} \\ -\sigma_y \hat{x} \end{pmatrix} \exp\left(-\hat{x}^2 - \hat{y}^2\right), \tag{2.3}$$
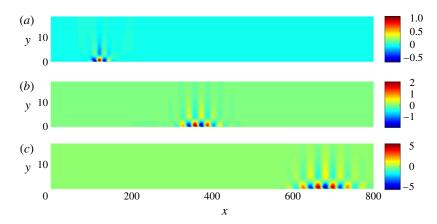
FIGURE 3. Streamwise component of the TS wave-packet generated as impulse response of the system to the perturbation $\boldsymbol{B}_w$. The snapshots are taken at three different instants of time: (*a*) $t = 200$, (*b*) 800, (*c*) 1600.

where

$$\hat{x} = \frac{x - x_0}{\sigma_x}, \quad \hat{y} = \frac{y - y_0}{\sigma_y}. \tag{2.4}$$

The scalar quantities $\sigma_x = 4$ and $\sigma_y = 1/4$ determine the size of the inputs, while the scalars x_0 and y_0 define the locations. Note that they are all of same size. From this definition, we obtain

$$\boldsymbol{B}_w = \boldsymbol{f}(x, x_w), \quad \boldsymbol{B}_u = \boldsymbol{f}(x, x_u), \tag{2.5}$$

with $\boldsymbol{x}_w = (35, 1)$ and $\boldsymbol{x}_u = (400, 1)$, see also figure 2. These positions are the same as already chosen by Bagheri *et al.* (2009*a*).

The sensor measurement $y(t)$ also incorporates a zero-mean Gaussian white noise $g(t)$, and is given by

$$y = \boldsymbol{C}_y \boldsymbol{q} + \eta g, \tag{2.6}$$

where η is the magnitude of the sensor noise, a parameter that is important for estimator design, to be discussed in §3.2. The performance measure $z(t)$ is given by the fictitious output

$$z = \begin{bmatrix} \boldsymbol{C}_z \\ \boldsymbol{0} \end{bmatrix} \boldsymbol{q} + \begin{bmatrix} 0 \\ l \end{bmatrix} u, \tag{2.7}$$

and is used to determine a cost function for the optimal control problem to be addressed in §3.1; in particular, the optimal controller will minimize $\|z\|_2$. The parameter l determines how much the control effort is penalized in the cost function and is referred to as the control penalty.

The flow measurements are obtained by averaging the velocity field over a small portion of the domain defined by the row vectors $\boldsymbol{C}_z$ and $\boldsymbol{C}_y$, defined from discretizations of the function (2.3) and used as weights. In particular,

$$\boldsymbol{C}_z \boldsymbol{q} = \int_{\Omega} \left(\boldsymbol{f}(x, x_z)^{\mathrm{T}} \boldsymbol{q} \right) \mathrm{d}x \, \mathrm{d}y, \quad \boldsymbol{C}_y \boldsymbol{q} = \int_{\Omega} \left(\boldsymbol{f}(x, x_y)^{\mathrm{T}} \boldsymbol{q} \right) \mathrm{d}x \, \mathrm{d}y, \tag{2.8}$$

where Ω indicates the computational domain. The output C_z is located at $x_z = (750, 1)$. Two different locations are chosen for the sensor C_y, see figure 2; the relative position along the streamwise direction of the actuator and sensor is important and influences the dynamics of the closed-loop system.

When the sensor is located downstream of the actuator, or a short distance upstream, it can measure the disturbance and the effect of the actuator; this configuration is referred to as *output feedback control*. If, on the other hand, the sensor is located far upstream of the actuator, it cannot measure the effect of the actuation, due to the strong advection dominating the flow. This configuration is a special case of output feedback control referred to as *disturbance feedforward control* in the framework described by Doyle *et al.* (1989); in this limit, the action of the controller is based only on the measurements of the disturbance $w(t)$. A straightforward way for testing the configuration is represented by the input–output analysis of the dynamics between the actuator B_u and the sensor C_y: feedback arises when the transfer function from u to y is non-zero.

Thus, it is possible to categorize the two configurations by analysing the behaviour of the signals in the time domain or the associated transfer function in the spectral domain. Note that feedback and feedforward controllers strongly differ in terms of stability properties and robustness to uncertainties of the system; these aspects are thoroughly analysed for the same configuration in Belson *et al.* (2013).

3. Optimal control and estimation: a brief review

The optimal control and the estimation problems are well known and the available literature is quite broad (see e.g. Lewis & Syrmos 1995; Zhou, Doyle & Glover 2002; Bagheri *et al.* 2009*b*); the aim of this section is to introduce the main relations in a concise way, as these will be needed in § 4.

3.1. *Full-information optimal control*

The heart of the optimal control problem is the minimization of the cost function

$$\mathscr{J}(q(u), u) = \frac{1}{2} \int_0^T \left(q^H Q_z q + u^H R u \right) \, \mathrm{d}t, \qquad (3.1)$$

where $Q_z \geqslant 0$ and $R > 0$ are weights that determine the relative penalties on the state perturbations $q(t)$ and control effort $u(t)$, respectively; the notation $(\cdot)^H$ denotes the conjugate transpose. Here, we choose $Q_z = C_z^H C_z$, and $R = l^2$, so the cost function is simply $\|z\|_{L^2[0,T]}^2$. Note that we have assumed that the cross-weighting between the state and the control term is null; this assumption does not lead to any loss of generality.

The optimal control $u(t)$ minimizes the cost $\mathscr{J}$ subject to the dynamics

$$\dot{q} = Aq + B_u u, \quad q(0) = q_0. \qquad (3.2)$$

Note that in the optimal control problem, the disturbance $w(t)$ is taken to be zero; however, this disturbance is needed in the optimal estimation problem. One way of solving this problem is to follow the Lagrangian approach, by forming an augmented cost function $\tilde{\mathscr{J}}$ based on the cost in (3.1) and equation (3.2), acting as constraint. The adjoint variable $p(t)$ corresponds to the Lagrangian multiplier and is governed by

$$\dot{p} = -A^H p - Q_z q, \quad p(T) = 0, \qquad (3.3)$$

where A^H denotes the adjoint operator. The adjoint operator satisfies the relation $\langle Aq, p \rangle = \langle q, A^H p \rangle$.

The optimal control is then given by

$$u(t) = -R^{-1}B_u^H p(t). \tag{3.4}$$

Introducing the linear dependence $p(t) = X(t)q(t)$, this solution may be written $u(t) = K(t)q(t)$, where

$$K(t) = -R^{-1}B_u^H X(t) \tag{3.5}$$

is the control gain $K(t) \in \mathbb{R}^{m \times n}$ and $X(t) \in \mathbb{R}^{n \times n}$ is a solution of a differential Riccati equation. In the limit as $T \to \infty$, X becomes a constant matrix, and is a positive-definite solution of an algebraic Riccati equation

$$A^H X + XA - XB_u R^{-1}B_u^H X + Q_z = 0. \tag{3.6}$$

Note that, for a given initial condition $q(0)$, the optimal input $u(t)$ may also be computed without Riccati equations by iteratively solving (3.2)–(3.3), together with the optimal condition (3.4) for a finite time-horizon T. In this case, the optimal input is computed using a gradient descent, noting that

$$\frac{\partial \tilde{\mathscr{J}}}{\partial u} = B_u^H p + Ru, \tag{3.7}$$

where $\tilde{\mathscr{J}}$ is the augmented cost function.

3.2. *Estimation problem and dual system*

In order to implement the feedback law $u(t) = Kq(t)$ from the previous section, one needs to know the flow state $q(t)$. However, in practice, only the sensor measurement $y(t)$ is available; thus, we replace $q(t)$ by a state estimate $\hat{q}(t)$, determined by an estimator that typically takes the form

$$\dot{\hat{q}} = A\hat{q} + B_u u - L(y - \hat{y}), \tag{3.8a}$$

$$\hat{y} = C_y \hat{q}. \tag{3.8b}$$

A stochastic framework is assumed for the description of the disturbance $w(t)$ and noise $g(t)$. As already mentioned, the terms $w(t)$ and $g(t)$ are modelled as white-noise stochastic processes with zero mean and known covariance matrices $W = \mathscr{E}\{ww^H\}$ and $G = \mathscr{E}\{gg^H\}$, respectively. The operator $\mathscr{E}(\cdot)$ indicates the expected value operator.

The estimator dynamics is forced by the last term proportional to the difference between the real measure $y(t)$ and the estimated measure $\hat{y}(t)$ via the matrix $L(t)$, referred to as estimation gain. The matrix $L(t)$ is designed to minimize the expected energy $Y = \mathscr{E}\{ee^H\}$ of the estimation error $e(t) = q(t) - \hat{q}(t)$, that satisfies the relation

$$\dot{e} = (A + LC_y)e + B_w w + \eta Lg, \tag{3.9}$$

obtained by combining (2.2) and the estimator (3.8). The gain $L(t) \in \mathbb{R}^{n \times p}$ assumes the form

$$L(t) = -Y(t)C_y^H G^{-1}, \tag{3.10}$$

where $Y(t) \in \mathbb{R}^{n \times n}$ is the solution of a second differential Riccati equation. Also in this case, in the limit $T \to \infty$, Y becomes a constant matrix, solution of the algebraic

Riccati equation associated with the estimation problem

$$AY + YA^H - YC_y^H G^{-1} C_y Y + B_w W B_w^H = 0. \tag{3.11}$$

Note that the unknown of the Riccati equation (3.11) is the expected energy of the estimation error $e(t)$ (Lewis & Syrmos 1995; Bagheri *et al.* 2009*b*).

By analogy with the control problem, it is interesting to note that the optimal gain matrix L can be computed by introducing the dual fictitious adjoint system

$$-\dot{p} = A^H p + C_y^H \tilde{y}, \quad p(T) = p_0, \tag{3.12}$$

where the 'feedback law' is now represented by $\tilde{y}(t) = L^H p(t)$. The dual system is defined by performing the adjoint of equation (3.9), governing the estimation error $e(t)$, where the disturbance $w(t)$ and the noise $g(t)$ are taken to be zero (Kim & Bewley 2007). Note that the adjoint of the outputs C_z^H and C_y^H are the inputs forcing in the dual adjoint system, while the adjoint of the inputs B_w^H and B_u^H plays the role of the outputs of the system (Kailath 1980; Bagheri *et al.* 2009*a*). Once the dual system is defined, one can cast a second optimization problem in order to minimize the auxiliary variable $p(t)$, based on the cost function

$$\mathcal{N}(p(\tilde{y}), \tilde{y}) = \frac{1}{2} \int_0^T \left(p^H Q_w p + \tilde{y}^H Q_g \tilde{y} \right) \, \mathrm{d}t. \tag{3.13}$$

The optimization procedure follows the same steps already outlined for the control problem: the Lagrangian multiplier $q(t)$ satisfies the relation

$$\dot{q} = Aq + Q_w p, \quad q(0) = 0, \tag{3.14}$$

while the associated gradient is

$$\frac{\partial \tilde{\mathcal{N}}}{\partial \tilde{y}} = C_y q + Q_g \tilde{y}. \tag{3.15}$$

Finally, the Riccati equation (3.11) is obtained by defining the matrices $Q_w = B_w W B_w^H$ and $Q_g = G$. Thus, also by following a 'deterministic' formulation for the estimation problem, the choice of the proper weights as covariance matrix allows us to recover the original stochastic connotation. Note that the matrix B_w enters the definition of Q_w, due to the input–output formulation.

3.3. *Linear quadratic Gaussian (LQG) controller*

Once the two optimal problems are solved, it is possible to show that the feedback gain can be applied to the estimated state $\hat{q}(t)$ in order to compute the control signal $u(t)$. The LQG controller can indeed be designed in these two steps, performed independently of each other (see Anderson & Moore 1990); according to the *separation principle*, if each of the two problems is stable, the final compensator, obtained from the optimal estimator and the optimal controller, will be stable and optimal. Thus, by combining the estimator (3.8) and the full-information controller in (3.5), we obtain the compensator or output feedback controller

$$\dot{\hat{q}} = \left(A + B_u K + L C_y \right) \hat{q} - L C_y q, \tag{3.16a}$$

$$u = K \hat{q}. \tag{3.16b}$$

Since the solution of the Riccati equation is a full matrix, the storage requirement is at least of $O(n^2)$. Moreover, the numerical methods for calculating the solution of

the Riccati equation are usually characterized by a computational complexity of $O(n^3)$, regardless of the structure of the system matrix A (Benner *et al.* 2008). Thus, the computation of the solution is too expensive for high-dimensional systems, $n > 10^3$. The reduce-then-design approach is usually adopted in the flow-control community (see e.g. Bagheri *et al.* 2009*b*). The controller is built by using a model able to capture the essential dynamics of the system. In the present investigation, the reduce-then-design strategy is compared with the full-dimensional LQG obtained by applying the iterative method outlined in the next section. The dynamical system in (3.16) runs next to the main DNS, either based on a reduced-order model or based on a second DNS when full-dimensional gains are used.

4. Optimization without Riccati equations

In Pralits & Luchini (2010), the adjoint of the direct-adjoint (ADA) algorithm for the solution of the control Riccati equation is introduced, starting from the classic direct-adjoint iteration. This direct-adjoint iteration for the optimal control problem allows us to determine the optimal control signal $u(t)$ for a given final time T, but it is not capable of computing the associated feedback gain K defined in (3.5). We summarize this method in § 4.1 and present the dual solution for an optimal estimator in § 4.2, following the same procedure.

4.1. *Adjoint of the direct-adjoint (ADA)*

For a given initial condition $q(0)$, the optimal input $u(t)$ may be computed without Riccati equations, by iteratively solving the direct equation (3.2) and the adjoint equation (3.3), and using a gradient descent to minimize the cost $\mathscr{J}$. When the iteration converges, i.e. $\partial \tilde{\mathscr{J}} / \partial u \to 0$, the optimality condition (3.4) holds. If we consider n linearly independent initial conditions (say, standard basis vectors of $\mathbb{R}^n$), then we may find the optimal input $u(t)$ for any initial condition $q(0)$, and compute the gain matrix K in (3.5). For instance, if one aims to compute the feedback gain in the limit as $T \to \infty$, i.e. when the solution is a constant matrix, it is possible to write

$$\begin{bmatrix} u_0^1 & u_0^2 & ... & u_0^n \end{bmatrix} = K(0) \begin{bmatrix} q_0^1 & q_0^2 & ... & q_0^n \end{bmatrix}, \tag{4.1}$$

and solve for the feedback gain matrix K at $t = 0$. When n is large, one such solution is feasible, but n solutions are clearly not feasible. However, if the resulting dimension of the outputs is much smaller than the degrees of freedom of the inputs, i.e. $n \gg m$, we may improve the situation by analysing the sensitivity with respect to the initial condition using the adjoint of the system (3.2)–(3.3), as elucidated by Pralits & Luchini (2010) and Bewley *et al.* (2012).

Letting $z = (p, q)$, equation (3.2) and the adjoint equation (3.3) can be arranged, together with the optimal condition $u(t) = -R^{-1}B_u^H p(t)$, into the following system

$$Tz = 0, \quad T = \begin{bmatrix} B_u R^{-1} B_u^H & \dfrac{\mathrm{d}}{\mathrm{d}t} - A \\ -\dfrac{\mathrm{d}}{\mathrm{d}t} - A^H & -Q_z \end{bmatrix}. \tag{4.2}$$

The initial conditions for the adjoint and direct equations are $q(0) = q_0$ and $p(T) = 0$, respectively. Note that the system is arranged in a slightly non-standard way by making the temporal derivative appear in the off-diagonal blocks of the operator, in order to simplify the following analysis. Now, we consider the variable $\tilde{z} = (\tilde{p}, \tilde{q})$. By

defining the inner product

$$\langle \boldsymbol{a}, \boldsymbol{b} \rangle = \int_0^T \boldsymbol{a}(t)^H \boldsymbol{b}(t) \, \mathrm{d}t, \tag{4.3}$$

one can express the following adjoint identity:

$$\langle \tilde{z}, \boldsymbol{T} z \rangle = \langle \boldsymbol{T}^H \tilde{z}, z \rangle + \boldsymbol{b}. \tag{4.4}$$

The last term in (4.4) is obtained via integration by parts and is

$$\boldsymbol{b} = \left. (\tilde{\boldsymbol{p}}^H \boldsymbol{q} - \tilde{\boldsymbol{q}}^H \boldsymbol{p}) \right|_0^T. \tag{4.5}$$

Now, suppose we solve the adjoint problem

$$\boldsymbol{T}^H \tilde{z} = 0, \qquad \begin{aligned} \tilde{\boldsymbol{q}}(0) &= \tilde{\boldsymbol{q}}_0, \\ \tilde{\boldsymbol{p}}(T) &= 0. \end{aligned} \tag{4.6}$$

It can be easily verified that equations (4.6) for the adjoint variable $\tilde{z}$ are identical to the original equations (4.2), that is $\boldsymbol{T} = \boldsymbol{T}^H$. If z is a solution of the original problem (4.2), then (4.4) and (4.5) together with the boundary conditions give

$$[\tilde{\boldsymbol{p}}(0)]^H \boldsymbol{q}(0) = [\tilde{\boldsymbol{q}}(0)]^H \boldsymbol{p}(0). \tag{4.7}$$

The optimality condition (3.4) can be imposed by comparing each row with the identity (4.7). In particular, noting that the gain matrix $\boldsymbol{K}(t)$ from (3.5) satisfies

$$\boldsymbol{K}(0)\boldsymbol{q}(0) = -\boldsymbol{R}^{-1} \boldsymbol{B}_u^H \boldsymbol{p}(0), \tag{4.8}$$

at $t = 0$, one sees that by introducing one row of the matrix $-\boldsymbol{R}^{-1} \boldsymbol{B}_u^H$ as initial condition $\tilde{\boldsymbol{q}}_0^H$, then the corresponding kth row of the optimal gain $\boldsymbol{K}(0)$ is given by $\tilde{\boldsymbol{p}}_0^H$ that results from the solution of (4.6). Thus, if the number of inputs is m, we can compute all m rows of $\boldsymbol{K}(0)$ from just m solutions of the adjoint problem (4.6), instead of n solutions of the original problem (4.2). In flow control, where usually $n \gg m$, this represents dramatic savings.

Thus, the computational machinery that one uses to solve (4.2) can be used for the ADA problem without modification, except the initial condition $\tilde{\boldsymbol{q}}_0$; however, due to the choice of the initial condition, the physical interpretation of the problem differs because it is no longer an optimal control problem for a given final time T.

In the limit as $t \to \infty$, the gain $\boldsymbol{K}(t)$ becomes a constant, equal to $\boldsymbol{K}(0)$, so this method recovers the standard infinite-time LQR solution. Thus, when the optimization is performed for a time interval T that is long enough, the ADA algorithm is capable of finding the exact solution of the Riccati problem.

4.2. *Adjoint of the adjoint-direct (AAD)*

As mentioned before, the machinery employed for the control problem can be adopted in an analogous manner for computing the full-dimensional estimation gain $\boldsymbol{L}$. The corresponding system consists of equation (3.12) for the adjoint state and the governing equation for the direct variable (3.14) which are arranged together with the optimal condition $\tilde{y}(t) = -\boldsymbol{Q}_g^{-1} \boldsymbol{C}_y \boldsymbol{q}(t)$ as

$$\tilde{\boldsymbol{T}} = \begin{bmatrix} \boldsymbol{C}_y^H \boldsymbol{Q}_g^{-1} \boldsymbol{C}_y & -\dfrac{\mathrm{d}}{\mathrm{d}t} - \boldsymbol{A}^H \\ \dfrac{\mathrm{d}}{\mathrm{d}t} - \boldsymbol{A} & -\boldsymbol{Q}_w \end{bmatrix}. \tag{4.9}$$

The initial conditions for the adjoint and direct equations are $p(0) = p_0$ and $q(-T) = 0$, respectively. In perfect analogy with the procedure already implemented for the control problem, the adjoint of the entire system together with the boundary conditions leads to the identity

$$[\tilde{q}(0)]^H p(0) = [\tilde{p}(0)]^H q(0). \tag{4.10}$$

By comparing the latter identity with the relation

$$[L(0)]^H p(0) = -Q_g^{-1} C_y q(0), \tag{4.11}$$

it is possible to note that by introducing one row of the matrix $-Q_g^{-1} C_y$ as initial condition $\tilde{p}_0^H$, the direct solution $\tilde{q}_0^H$ at time $t = 0$ provides the corresponding row of $[L(0)]^H$, once the iteration is converged.

In conclusion, the full-dimensional LQG compensator in (3.16) can be computed by combining the AAD solutions for the computation of the estimation gains, L, and the ADA solutions for the controller gains, K.

4.3. *Implementation and convergence*

The algorithm for computing the full-dimensional gains is based on a classic iteration where each step consists of a forward direct numerical simulation followed by the associated adjoint simulation that marches the system backwards in time (see e.g. Schmid 2007, and the references contained therein). For sake of clarity, we sketch the iteration in the following, by using the ADA algorithm as an example.

(*a*) First, (3.2) is solved by marching the time stepper forward it time until T; the cost function $\mathscr{J}$ can be estimated by using the integral in (3.1).

(*b*) Equation (3.3) is solved backwards in time. A modified version of the time stepper is used, where the adjoint equations are implemented. For the derivation of this set of equations, we refer to Bagheri *et al.* (2009*a*). Note that the forcing term consists of the full state of (3.2); thus, in general, a proper implementation should include a checkpoint procedure for the storage of the flow fields $q \in [0, T]$. However, due to the input–output configuration, the term $Q_z = C_z^H C_z$ appearing on the right-hand side of (3.3) is low-rank; thus, it is sufficient to compute the output signal $z = C_z q$ and force the adjoint solution by introducing this signal as input of the forcing via C_z^H. In fact, the output of the direct problem plays the role of input in the adjoint system. For the estimation problem, the corresponding term is $Q_w = B_w W B_w^H$ (see (3.14)).

(*c*) Finally the control signal $u(t)$ is updated at each iteration by minimizing the cost function $\mathscr{J}$ via a conjugate-gradient method (see e.g. Press *et al.* 2007). The control signal is computed as

$$u^{i+1} = u^i + \alpha^i h^i. \tag{4.12}$$

A line-minimization algorithm is used for the computation of α^i in (4.12), based on Brent's method outlined by Press *et al.* (2007). The signal $u(t)$ is taken to be zero as guess for the first iteration, while the direction h^i is initialized as $h^1 = -g^1$. The gradient g^i is computed using (3.7). The first term of the gradient corresponds to the output of the adjoint system, while the second term is given by the control signal $u(t)$. At each iteration the direction h^i is updated using the gradient g as

$$h^i = -g^i + \beta^i h^{i-1}. \tag{4.13}$$

Input: Initial guess at $i = 1$, u on $t \in [0, T]$
              Initial condition $\boldsymbol{q}_0$, corresponding to the kth row of $-\boldsymbol{R}^1 \boldsymbol{B}_u^H$
              Tolerance ε

1:   Solve $\mathrm{d}\boldsymbol{q}/\mathrm{d}t = \boldsymbol{A}\boldsymbol{q} + \boldsymbol{B}_u u$,   with $\boldsymbol{q}(0) = \boldsymbol{q}_0$, solved forward in time for $t \in [0, T]$
2:   Compute $\mathscr{J} = \mathscr{J}(\boldsymbol{q}(u), u)$
3:   **if** $i > 0$ and $(\mathscr{J}^{i+1} - \mathscr{J}^i)/\mathscr{J}^i < \varepsilon$, **then**
        exit loop
   end if
4:   Solve $\mathrm{d}\boldsymbol{p}/\mathrm{d}t = -\boldsymbol{A}^H \boldsymbol{p} - \boldsymbol{Q}_z \boldsymbol{q}$,   with $\boldsymbol{p}(T) = 0$, solved backwards in time for $t \in [0, T]$
5:   Compute $\partial \tilde{\mathscr{J}}/\partial u = \boldsymbol{B}_u^H \boldsymbol{q} + \boldsymbol{R} u$
6:   Update u via gradient-based method (see §4.3)
7:   **go to** 1

Output: kth row of the control gain $\boldsymbol{K}$, corresponding to $\boldsymbol{p}_0$ at $t = 0$

TABLE 1. Adjoint of direct-adjoint (ADA) algorithm.

The coefficient β^i is computed using the Fletcher–Reeves formula. An alternative method, steepest descent, has been successfully used by Pralits & Luchini (2010).

The ADA algorithm is summarized in table 1. The dual scheme is adopted for the AAD iteration by applying the relations reported in §§ 3.2 and 4.2. In this case, an adjoint-direct iteration is performed; at each step of the iteration, the governing equation (3.12) is marched backwards in time, forced by the 'control' signal $\tilde{y}(t)$, while equation (3.14) is marched forward in time. The gradient is computed using (3.15).

The convergence is analysed by considering the cost $\mathscr{J}$, the norm of the gradient $\partial \tilde{\mathscr{J}}/\partial u$ and the final time of optimization T.

The first two parameters are related to the convergence of the method, given a certain tolerance; as convergence criterion, the relative error $\delta \mathscr{J} = (\mathscr{J}^{i+1} - \mathscr{J}^i)/\mathscr{J}^i$ has been chosen, while the norm of the cost-gradient $\|\partial \tilde{\mathscr{J}}/\partial u\|$ needs to decrease when the iteration is progressing. The corresponding parameters are used for the AAD algorithm by processing the cost function value $\mathscr{N}$ and the norm $\|\partial \tilde{\mathscr{N}}/\partial \tilde{y}\|$, while the iteration advances. In figure 4, these parameters are shown as a function of the number of iterations. Figure 4(a,b) shows the convergence rate of three different control gains $\boldsymbol{K}$, characterized by control penalty $l^2 = [50, 100, 500]$. The algorithm is used with a tolerance value of $\varepsilon = 1.0 \times 10^{-8}$, which is deemed sufficient to guarantee converged results. The required number of iterations varies with the control penalty l; in particular, the convergence of the algorithm slows down when l is decreased. The results in figure 4(a,b) are associated with a final time $T = 2600$. From the theoretical point of view, this parameter is particularly interesting: the solution of the optimization procedure has to be independent of the final time of the simulations. Thus, the optimization time needs to be long enough in order to provide the exact solution of the Riccati equation. As a starting guess, T is chosen as the time required for a wave-packet produced at the initial-condition location to be convected out of the computational domain. A convergence test can be performed efficiently by taking the initial guess for $u(t)$ to be the final result from a computation with a shorter value of T, and extrapolating it for a longer time window.
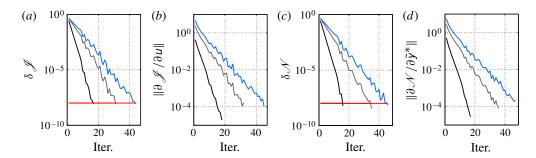
FIGURE 4. Convergence of the ADA algorithm (*a,b*) and AAD algorithm (*c,d*). (*a*) The convergence of the cost function $\mathscr{J}$ is shown by considering the relative error $\delta\mathscr{J}$ between two successive iterations; three control penalties are considered: $l^2 = 500$ (black solid line), $l^2 = 100$ (grey solid line) and $l^2 = 50$ (blue solid line). The red solid line indicates the chosen tolerance. The final time of integration for each direct-adjoint iteration is $T = 2600$. In (*b*), the 2-norm of $\partial\tilde{\mathscr{J}}/\partial u$ is shown as a function of the iterations (same legend as in *a*). For the AAD algorithm, $\delta\mathscr{N}$ is shown in (*c*) and the 2-norm of $\partial\tilde{\mathscr{N}}/\partial\tilde{y}$ in (*d*), for the cases $\eta^2 = 500$ (black solid line), $\eta^2 = 100$ (grey solid line) and $\eta^2 = 50$ (blue solid line). The final time of integration is $T = 2200$.

The convergence features of the AAD algorithm are similar (see figure 4*c,d*); the estimation gain L associated with a sensor located at $x_y = 300$ is analysed, for three different values $\eta = [50, 100, 500]$ and a final time $T = 2200$. Also for the AAD algorithm, the number of iterations increases progressively, when reducing the scalar value η; in general, for the case analysed in this paper, it is possible to get converged results within a number of iterations of $O(100)$ (at most).

As already mentioned, each iteration includes a line-minimization (Press *et al.* 2007); thus, the total number of adjoint-direct (direct-adjoint) simulations used is actually larger than the number of iterations, because the value of the cost $\mathscr{J}$ ($\mathscr{N}$) is evaluated more than once for every iteration step.

4.3.1. *Control and estimation gains*

In figure 5(*a,b*) the streamwise component of the estimation gains obtained are shown for two different positions of the estimation sensor C_y, here indicated by a region denoted by a darker stripe. The solution is obtained from the direct problem and resembles a TS wave-packet located just upstream of the sensor location; the gains are characterized by a compact spatial support. The spatial distribution of the gains L can also be justified by considering the related Riccati equation (3.11) and the definition (3.10); the estimation problem depends on the location and spatial distribution of the disturbance B_w and sensor C_y, and the covariances W and G of the excitation and sensor noise, but it does not depend on a final state that needs to be achieved, as it does for the control problem. Thus, the spatial support of the gain is mainly confined between the locations of B_w and C_y. The penalty $\eta = 1$, for all the cases treated in this paper. Different locations were tested for the sensor C_y, in the range $x_y = [250, 600]$; in all the cases, the gains L are characterized by similar features.

The control gain K is obtained as the solution of the adjoint equation, see figure 5(*c,d*). The spatial distribution is characterized by the typical tilted shape leaning against the direction of the shear. In figure 5(*c*) the control gain K associated
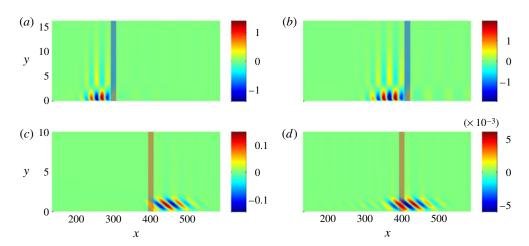
FIGURE 5. (*a,b*) Estimation gain L with $\eta^2 = 1$, for two different positions of the sensor C_y, here indicated by a darker stripe, $x_y = 300$ (*a*) and $x_y = 405$ (*b*). (*c,d*) The control gain K for the actuator B_u located at $x_u = 400$. The control penalty of the gains is $l^2 = 1$ (*c*) and $l^2 = 500$ (*d*). For all of them the streamwise component is depicted.

with the actuator location $x_u = 400$ and $l^2 = 1$ is shown; the packet is localized downstream of the actuator and is characterized by a compact support. In figure 5(*d*), the control gain associated with the same configuration and $l^2 = 500$ is depicted. As expected, the magnitude of the gains decreases; moreover, the spatial distribution is slightly different and also extends upstream of the actuator location.

4.3.2. *Controller reduction on a basis of balanced modes*

Figure 6 shows the estimation and controller gains when projected on a basis of $r = 80$ modes. The chosen basis $\boldsymbol{\Phi} \in \mathbb{R}^{n \times r}$ is composed by an approximate balanced mode, used in combination with the related adjoint base $\boldsymbol{\Psi} \in \mathbb{R}^{r \times n}$ for generating a reduced-order model of the system (Rowley 2005). The modes are obtained by collecting snapshots from the impulse response of the system to each input, by using forward simulations, and each output, by using adjoint simulations. The reduced gains are obtained as $\hat{\boldsymbol{K}} = \boldsymbol{K} \boldsymbol{\Phi}$ and $\hat{\boldsymbol{L}} = \boldsymbol{\Psi} \boldsymbol{L}$. A perfect matching is found between the gains obtained by following the design-then-reduce strategy and the reduce-then-design scheme adopted in Bagheri *et al.* (2009*a*). For this reason, in the next section, the controllers based on full-dimensional methods (FD) are compared with those obtained by designing the controller based on reduced-order models (RM). The models are obtained by performing a Galerkin projection over the balanced modes basis.

5. Results

In this section, the optimal control and estimation gains are used in combination with the time stepper in order to simulate a flow compensated by the LQG controller. The closed loop is obtained by coupling two different versions of the code: the main DNS of the perturbation flow according to (3.2) to a second one that marches forward in time the dynamical system (3.16).

The effects of the controller can be qualitatively considered by observing the evolution of the wave-packet in physical space when the control is active. In figure 7,
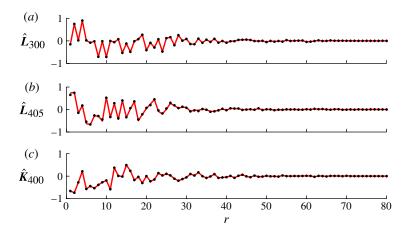
FIGURE 6. Reduced-order gains; $\hat{L}$ is shown for two different positions of the sensor C_y at $x_y = 300$ (*a*) and $x_y = 405$ (*b*), while $\hat{K}$ is shown for the actuator location $x_u = 400$ (*c*). The gains obtained by following the design-then-reduce approach (red solid line) are perfectly in agreement with the gains obtained by first reducing the model and then designing the controller (black dots).
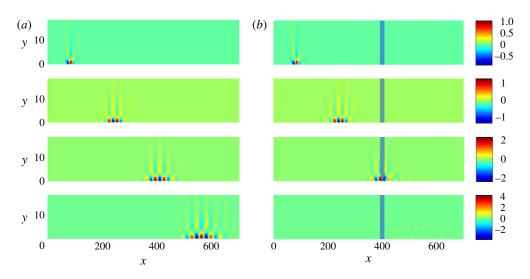

FIGURE 7. Evolution of an uncontrolled wave-packet (*a*) compared to a controlled case (*b*) for four different instants of time, $t = [100, 500, 900, 1300]$, from top to bottom. The streamwise component is shown with the same contour level at each instant of time; the blue stripe in (*b*) indicates the location of the actuator B_u, $x_u = 400$.

the uncontrolled configuration is compared with a controlled case where a feedforward setup is considered with $x_y = 300$, and control penalty $l^2 = 50$; four different instants of time are shown. The actuator is located at $x_u = 400$ and starts to damp the wave-packet while it propagates downstream. Once the controller has successfully damped the wave-packet, a strong reduction of the energy amplitude can be observed (see figure 8*e*).
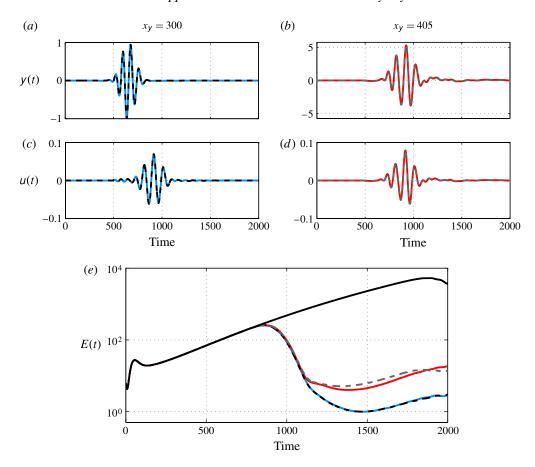
FIGURE 8. Input–output dynamics for two different control configurations. The estimation signal y and the control $u(t)$ are depicted in (a) and (c), respectively, for the feedforward configuration, and in (b) and (d), respectively, for the feedback configuration. The perturbation energy as a function of time is shown in (e), compared to the uncontrolled case (black solid line). For all figures: the full-dimensional (FD) case $x_y = 300$ is indicated by a blue solid line, the FD case $x_y = 405$ by a red solid line, the reduced-order model (RM) case $x_y = 300$ by a black dashed line and the RM case $x_y = 405$ by a grey dashed line.

In the following, a quantitative analysis of the results is provided by comparing the input–output dynamics, the energy evolution in time of the perturbation and the cost value. Full-dimensional controllers are compared with the corresponding case where model reduction is used; moreover, the finite-amplitude case is discussed for different typologies of controllers when using the full-dimensional gains.

In figure 8 we report a comparison between the performance achieved with the FD controller and the RM for the two configurations introduced in §2.1. The controller where $x_y = 300$ is considered in figure 8(a,c). The setup is in feedforward configuration; the dynamics between sensor $\boldsymbol{C}_y$ and actuator $\boldsymbol{B}_u$ is negligible. The perfect agreement characterizing the estimated signal $y(t)$ in figure 8(a) and the control signal $u(t)$ shown in figure 8(c), when comparing FD and RM methods, leads to the same behaviour for the compensated flow when the perturbation energy $E(t) = \langle \boldsymbol{q}, \boldsymbol{q} \rangle$ is analysed as a function of time (figure 8e). Feedforward configurations

x_y	Case	l^2	$\mathscr{J}_{FD}$	$\mathscr{J}_{RM}$
		1	0.610	0.627
300	FFW	50	17.617	17.629
		100	33.051	33.060
		1	2.123	2.812
405	FBK	50	19.956	20.491
		100	36.694	37.005
		1	4.222	—
415	FBK	50	29.904	29.974
		100	51.650	51.613

TABLE 2. Control cost for three different configurations. The labels FFW and FBK indicate the feedforward and feedback cases, respectively; l is the control gain, $\mathscr{J}_{FD}$ is the cost for the full-dimensional cases, $\mathscr{J}_{RM}$ is the cost for the reduced-order model cases.

are not affected by a small error in approximating the plant. Conversely, when a feedback configuration is considered, instabilities of the closed loop can be an issue (see Belson *et al.* 2013).

5.1. *Reduce-then-design versus full-dimensional controllers*

The estimation signal $y(t)$ and the control signal $u(t)$ are shown in figure 8(*a–d*); the agreement is fairly good as revealed by a qualitative inspection of the perturbation energy curve in figure 8(*e*), even though the match between the two cases is not as good as in the feedforward case where the two results are barely distinguishable. From the quantitative point of view, the good agreement between RM and FD is confirmed by the values of the cost function $\mathscr{J}$ (see table 2). Also in this case, a perfect match is found when feedforward configurations are considered, while for the feedback configuration we observe a small deviation in the results, and – more interestingly – for positions of the sensor further downstream of the actuator, $x_y \geqslant 415$, the model-reduction control does not guarantee stability of the closed loop. An example is provided by the results shown in table 2: when strong actuation ($l^2 = 1$) is chosen for the feedback control with $x_y = 415$, the controller becomes unstable. The stability of the closed loop was also investigated by varying the size of the reduced-order model r when performing the Galerkin projection, but without observing any improvements in the dynamics of the closed-loop system.

A physical explanation can be found by considering that an open-loop model reduction is performed, where the most observable and controllable states are ranked for obtaining a reduced-order model without accounting for the effects of the actuation. In a feedforward configuration, this modelling procedure is enough to guarantee stability of the controller; indeed, the closed-loop system is inherently an open-loop system, where the actuation effects are never fed back into the controller system. Vice versa, when the controller is in feedback configuration, the estimation sensor can measure the effects of the actuation, but the resulting model may not be sufficient for the design of the controller in these conditions. This observation is supported by the efficiency of the full-dimensional design that is able to guarantee stability when changing the position of the sensor and tuning the control penalty l. In control literature, this condition is usually referred to as the *spill-over* effect and it is a rather typical condition when open-loop model reduction is applied for the control of a full

plant. By considering the results of the gains projection shown in §4.3.2, it is possible to argue that a basis that also includes the effects of the actuation might lead to an improvement of the closed-loop system when the configuration is not degenerating in a feedforward case (Losse *et al.* 2011).

Higher values of l^2, corresponding to weaker action of the controller, result in stable closed loop for both of the analysed methodologies. Configurations based on a sensor upstream of the actuator are characterized by better performance in terms of perturbation amplitude reduction. Cases where the estimation sensor is located downstream of the actuator show a progressive decay of the performance. Nonetheless, a sensor downstream of the actuator is of interest for such a flow case strongly dominated by the advection, whenever we are interested in a configuration truly characterized by a feedback dynamics or based on adaptive controllers, as often found in experiments (see e.g. Sturzebecher & Nitsche 2003). In that sense, locations relatively far from the actuator are also of practical interest, because of the constraints arising in the implementation of the control hardware (the geometry of the actuator, for instance).

In conclusion, the reduce-then-design scheme based on an open-loop model reduction might be limiting, as shown by the comparison carried out in this section. This discussion does not apply when the output feedback controller degenerates into the limit of a feedforward controller, i.e. a controller inherently resulting in an open-loop compensator.

5.2. *Effect of the nonlinearities*

The limitations of the linear optimal controllers when finite-amplitude perturbations are introduced in full nonlinear DNS (Chevalier *et al.* 2007*b*) can be analysed using the full-dimensional gains by decoupling the effects of the linear controller when nonlinearities are present in the flow from the role of the estimation. Indeed, the full-information control can be used once the full-dimensional gain K is available. In figure 9, the perturbation energy behaviour as a function of time is shown for two different cases characterized by different initial amplitudes, by defining the amplitude of the perturbation $q(t)$ as

$$a(t) = \left(\max_{x,y} q\,(t) - \min_{x,y} q\,(t) \right) /2U_\infty. \tag{5.1}$$

In figure 9(*a*) the case with $a_0 = 0.30\,\%$, is shown while higher amplitudes up to $a_0 = 1.52\,\%$ are analysed in figure 9(*b*). The red solid line indicates for both cases the results obtained by a linear quadratic regulator (LQR), with control penalty $l^2 = 50$. Note that the performance of the LQR does not depend on the initial condition used for the disturbance: in the control Riccati equation (3.6) the input triggering the disturbance does not appear while we require knowledge of the actuator B_u, the objective function C_z – hidden in the last term Q_z – and the system matrix A. Numerical simulations were performed with initial disturbance placed at different locations along the streamwise coordinate. When the resulting spatial support of the incoming disturbance is upstream of the spatial distribution of the controller gain K (see figure 5) is always possible to achieve good performance within the linear limit and weakly nonlinear case. Thus, the limitations are mostly related to the choice of the actuator and – more importantly when nonlinear cases are tested – the accuracy of the model used for the control design (i.e. the linearized Navier–Stokes). These results represent the lower bound for the performance of such a controller designed for a localized actuator by using linear approximation and for a given initial,
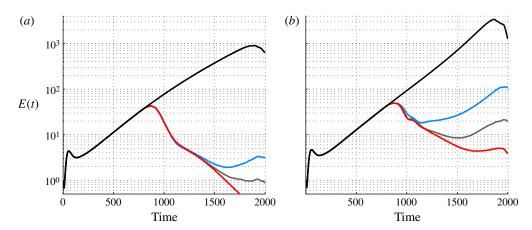
FIGURE 9. Perturbation energy as a function of time. In (*a*), the initial amplitude $a = 0.30\,\%$, while in (*b*) $a = 1.52\,\%$. The red solid line indicates the performance achieved by using an LQR, the grey solid line an LQG with nonlinear estimator and the blue line an LQG with linear estimator. Black solid line indicates the reference case without control.

finite, amplitude of the perturbation. In other words, a control design based on these 'ingredients' cannot perform better; thus, the full-dimensional LQR controller results in a benchmark for the performance that it is possible to achieve.

When a linear estimator is introduced, as expected, a degrading of the performance is observed: the evolution of the propagating wave-packet starts to diverge from the linearized one due to the presence of the nonlinearities in the flow. For this case, a feedforward configuration with $x_y = 300$ is chosen. Higher amplitudes are characterized by stronger deviation: considering the cost function $\mathscr{J}$ for the case in figure 9(*a*), an increase of 6.3 % is observed while for the case in figure 9(*b*) the worsening is of order 70 %. The corresponding energy curve (green solid line in the plot) shows more than one order of magnitude of difference for the latter case. Note that when the reduced-order-model-based LQG is employed, the results perfectly match the full-dimensional LQG.

When the estimation gains designed in the linear limit are used in combination with an estimator based on the full Navier–Stokes equations, similarly to what happens when the extended Kalman filter is applied, the decay of the performance is significantly reduced. Thus, also for this case, full-dimensional gains can serve as a benchmark for comparing the performance of a reduced-order-model-based controller with nonlinear effects included with the best performance achievable by using a perfect estimator based on the full model. Note, however, that while the case represented by the LQR is a lower bound for the control performance depending on the actuator, the control penalty chosen during the design and the system matrix, the estimator for the nonlinear cases is strongly affected by the location of the sensor along the streamwise direction, due to the increasing amplitudes of the disturbance and the mechanisms triggered by the nonlinearities, and the disturbance modelled by $\boldsymbol{B}_w$.

6. Concluding remarks

The attenuation of Tollmien–Schlichting (TS) waves in a two-dimensional boundary layer, by using full-dimensional controllers based on optimal controllers/estimators, was investigated by means of direct numerical simulations.

The *adjoint of the direct-adjoint* (ADA) algorithm for the solution of optimal control problems, first introduced by Pralits & Luchini (2010), was extended to the estimation problem by using the dual adjoint system. In the present contribution, the algorithm has been referred to as *adjoint of adjoint-direct* (AAD).

The two approaches were applied for the design of full-dimensional linear quadratic Gaussian (LQG) controllers in a two-dimensional boundary layer developing over a flat plate. The configuration was the same as used by Bagheri *et al.* (2009*a*), where the controllers were designed using a reduced-order model; such a strategy is referred to as reduce-then-design in the literature (Anderson & Liu 1989) and is the usual approach followed in the flow-control community for the treatment of such large-scale systems (Bagheri *et al.* 2009*b*).

The full-dimensional LQG was taken as benchmark for two different analyses. First, the relative position between estimation sensor and actuator was tested. A good agreement over a wide range of parameters, including the number of modes for the Galerkin projection and the penalty gains, was found between the controllers designed by using a reduced-order model, and the full-dimensional controllers when a disturbance feedforward configuration (Doyle *et al.* 1989) for the estimator sensor placement was used. However, when the estimator sensor was introduced in feedback configuration, only the full-dimensional methods guarantee stability over a broad range of parameters, including the sensor placement along the streamwise direction and control penalty gains. Vice versa, controllers based on open-loop model reduction were not able to always guarantee stability of the controlled system.

Finite-amplitude disturbances were also analysed with the aim of detecting the decay of the performance due to the effects of the nonlinearities. For this case, the optimal controller based on the full state can be considered as a lower bound for the achievable performance. When considering a controller based on an estimator, the full-dimensional gains allow one to analyse the ideal case of a fully nonlinear estimator.

Acknowledgements

REFERENCES

ABERGEL, F. & TEMAM, R. 1990 On some control problems in fluid mechanics. *Theor. Comput. Fluid Dyn.* **1**, 303–325.

ÅKERVIK, E., HŒPFFNER, J., EHRENSTEIN, U. & HENNINGSON, D. S. 2007 Optimal growth, model reduction and control in a separated boundary-layer flow using global eigenmodes. *J. Fluid Mech.* **579**, 305–314.

AKHTAR, I., BORGGAARD, J., STOYANOV, M. & ZIETSMAN, L. 2010 On commutation of reduction and control: linear feedback control of a von Kármán Street. In *5th Flow Control Conference*, pp. 1–14. American Institute of Aeronautics and Astronautics.

ANDERSON, B. & LIU, Y. 1989 Controller reduction: concepts and approaches. *IEEE Trans. Autom. Control* **34**, 802–812.

ANDERSON, B. & MOORE, J. 1990 *Optimal Control: Linear Quadratic Methods*. Prentice Hall.

BAGHERI, S., BRANDT, L. & HENNINGSON, D. S. 2009*a* Input–output analysis, model reduction and control design of the flat-plate boundary layer. *J. Fluid Mech.* **620**, 263–298.

BAGHERI, S., HŒPFFNER, J., SCHMID, P. J. & HENNINGSON, D. S. 2009*b* Input–output analysis and control design applied to a linear model of spatially developing flows. *Appl. Mech. Rev.* **62** (2), 020803.

BAMIEH, B., PAGANINI, F. & DAHLEH, M. 2002 Distributed control of spatially invariant systems. *IEEE Trans. Autom. Control* **47** (7), 1091–1107.

BANKS, H. T. & ITO, K. 1991 A numerical algorithm for optimal feedback gains in high dimensional linear quadratic regulator problems. *SIAM J. Control Optim.* **29** (3), 499–515.

BECHERT, D. & BARTENWERFER, M. 1989 The viscous flow on surfaces with longitudinal ribs. *J. Fluid Mech.* **206**, 105–129.

BELSON, B. A., SEMERARO, O., ROWLEY, C. W. & HENNINGSON, D. S. 2013 Feedback control of instabilities in the two-dimensional Blasius boundary layer: the role of sensors and actuators. *Phys. Fluids* **25**, 054106.

BENNER, P. 2004 Solving large-scale control problems. *Control Systems IEEE* **24** (1), 44–59.

BENNER, P., LI, J. & PENZL, T. 2008 Numerical solution of large-scale Lyapunov equations, Riccati equations, and linear-quadratic optimal control problems. *Numer. Linear Algebra Appl.* **15**, 755–777.

BEWLEY, T. R. 2001 Flow control: new challenges for a new renaissance. *Prog. Aerosp. Sci.* **37**, 21–58.

BEWLEY, T., LUCHINI, P. & PRALITS, J. 2012 Methods for the solution of large optimal control problems that bypass open-loop model reduction. *IEEE Trans. Autom. Control* (submitted).

BEWLEY, T. R., MOIN, P. & TEMAM, R. 2001 DNS-based predictive control of turbulence: an optimal benchmark for feedback algorithms. *J. Fluid Mech.* **447**, 179–225.

BEWLEY, T., PRALITS, J. & LUCHINI, P. 2007 Minimal-energy control feedback for stabilization of bluff-body wakes based on unstable open-loop eigenvalues and left eigenvectors. In *5th Conference on Bluff Body Wakes and Vortex-Induced Vibrations (BBVIV-5), 12-15 December, Bahia, Brazil.*

BORGGAARD, J. & STOYANOV, M. 2008 An efficient long-time integrator for Chandrasekhar equations. In *47th IEEE Conference on Decision and Control*, pp. 3983–3988. IEEE.

CHEVALIER, M., HŒPFFNER, J., ÅKERVIK, E. & HENNINGSON, D. S. 2007*a* Linear feedback control and estimation applied to instabilities in spatially developing boundary layers. *J. Fluid Mech.* **588**, 163–187.

CHEVALIER, M., SCHLATTER, P., LUNDBLADH, A. & HENNINGSON, D. S. 2007*b* A pseudo spectral solver for incompressible boundary layer flows, Trita-Mek 7. KTH Mechanics, Stockholm, Sweden.

CHOI, H., MOIN, P. & KIM, J. 1993 Direct numerical simulation of turbulent flow over riblets. *J. Fluid Mech.* **255**, 503–539.

CORBETT, P. & BOTTARO, A. 2001 Optimal control of nonmodal disturbances in boundary layers. *Theor. Comput. Fluid Dyn.* **15** (2), 65–81.

DOYLE, J. C., GLOVER, K., KHARGONEKAR, P. P. & FRANCIS, B. A. 1989 State-space solutions to standard H_2 and H_∞ control problems. *IEEE Trans. Autom. Control* **34**, 831–847.

HAMMOND, E. P., BEWLEY, T. R. & MOIN, P. 1998 Observed mechanisms for turbulence attenuation and enhancement in opposition-controlled wall-bounded flows. *Phys. Fluids* **10** (9), 2421–2423.

HERVÉ, A., SIPP, D., SCHMID, P. J. & SAMUELIDES, M. 2012 A physics-based approach to flow control using system identification. *J. Fluid Mech.* **702**, 26–58.

HÖGBERG, M., BEWLEY, T. R. & HENNINGSON, D. S. 2003 Linear feedback control and estimation of transition in plane channel flow. *J. Fluid Mech.* **481**, 149–175.

ILAK, M. & ROWLEY, C. W. 2008 Modelling of transitional channel flow using balanced proper orthogonal decomposition. *Phys. Fluids* **20**, 034103.

JUANG, J. & PAPPA, R. S. 1985 An eigensystem realization algorithm for modal paramter identification and model reduction. *J. Guid. Control Dyn.* **3** (25), 620–627.

KAILATH, T. 1980 *Linear Systems*. Prentice-Hall.

KIM, J. & BEWLEY, T. R. 2007 A linear systems approach to flow control. *Annu. Rev. Fluid Mech.* **39**, 383–417.

LEWIS, F. L. & SYRMOS, L. V. 1995 *Optimal Control*. John Wiley & Sons.

LOSSE, N. R., KING, R., ZENGL, M., RIST, U. & NOACK, B. R. 2011 Control of Tollmien–Schlichting instabilities by finite distributed wall actuation. *Theor. Comput. Fluid Dyn.* **25** (1–4), 167–178.

LUCHINI, P., MANZO, F. & POZZI, A. 1991 Resistance of a grooved surface to parallel flow and cross-flow. *J. Fluid Mech.* **228**, 87–109.

MA, Z., AHUJA, S. & ROWLEY, C. W. 2011 Reduced order models for control of fluids using the eigensystem realization algorithm. *Theor. Comput. Fluid Dyn.* **25** (1–4), 233–247.

MONOKROUSOS, A., BRANDT, L., SCHLATTER, P. & HENNINGSON, D. S. 2008 DNS and LES of estimation and control of transition in boundary layers subject to free stream turbulence. *Intl J. Heat Fluid Flow* **29** (3), 841–855.

MOORE, B. 1981 Principal component analysis in linear systems: controllability, observability, and model reduction. *IEEE Trans. Autom. Control* **26** (1), 17–32.

NORDSTRÖM, J., NORDIN, N. & HENNINGSON, D. S. 1999 The fringe region technique and the Fourier method used in the direct numerical simulation of spatially evolving viscous flows. *SIAM J. Sci. Comput.* **20** (4), 1365–1393.

PRALITS, J. O. & LUCHINI, P. 2010 Riccati-less optimal control of bluff-body wakes. In *Seventh IUTAM Symposium on Laminar–Turbulent Transition* (ed. P. Schlatter & D. S. Henningson), vol. 18. Springer.

PRESS, W. H., TEUKOLSKY, S. A., VETTERLING, W. T. & FLANNERY, B. P. 2007 *Numerical Recipes: The Art of Scientific Computing*, 3rd edn. Cambridge University Press.

QUADRIO, M. & RICCO, P. 2004 Critical assessment of turbulent drag reduction through spanwise wall oscillations. *J. Fluid Mech.* **521**, 251–271.

ROWLEY, C. W. 2005 Model reduction for fluids using balanced proper orthogonal decomposition. *Intl J. Bifurcation Chaos* **15** (3), 997–1013.

ROWLEY, C. & JUTTIJUDATA, W. 2005 Model-based control and estimation of cavity flow oscillations. In *44th IEEE Conference on Decision and Control*, pp. 512–517. IEEE.

SCHMID, P. J. 2007 Nonmodal stability theory. *Annu. Rev. Fluid Mech.* **39**, 129–162.

SCHMID, P. J. & HENNINGSON, D. S. 2001 *Stability and Transition in Shear Flows*. Springer.

SEMERARO, O., BAGHERI, S., BRANDT, L. & HENNINGSON, D. S. 2011 Feedback control of three-dimensional optimal disturbances using reduced-order models. *J. Fluid Mech.* **677**, 63–102.

STURZEBECHER, D. & NITSCHE, W. 2003 Active cancellation of Tollmien–Schlichting waves instabilities on a wing using multi-channel sensor actuator systems. *Intl J. Heat Fluid Flow* **24**, 572–583.

WHITE, E. & SARIC, W. 2000 Application of variable leading-edge roughness for transition control on swept wings. *AIAA Paper* 2000-283.

ZHOU, K., DOYLE, J. C. & GLOVER, K. 2002 *Robust and Optimal Control*. Prentice Hall.